Applied Catalysis B: Environmental 91 (2009) 546–553

Contents lists available at ScienceDirect

Applied Catalysis B: Environmental

journal homepage: www.elsevier.com/locate/apcatb

$M/TiO_2/SiO_2$ (M = Fe, Mn, and V) catalysts in photo-decomposition of sulfur mustard

Ştefan Neaţu [a], Vasile I. Pârvulescu [a,*], Gabriel Epure [b], Nicoleta Petrea [b], Vasile Şomoghi [b], Gabriele Ricchiardi [c], Silvia Bordiga [c,1], Adriano Zecchina [c,1]

[a] University of Bucharest, Faculty of Chemistry, Department of Chemical Technology and Catalysis, Bd. Regina Elisabeta 4–12, 030018, Bucharest, Romania
[b] Chemical Centre for Defence NBC and Ecology, Sos. Oltenitei 225, 041309, Bucharest, Romania
[c] University of Turin, Department of Chemistry IFM and NIS-Centre of Excellence, Via P. Giuria 7, 10125, Turin, Italy

ARTICLE INFO

Article history:
Received 30 April 2009
Received in revised form 19 June 2009
Accepted 20 June 2009
Available online 26 June 2009

Keywords:
Photocatalysis
Titania-silica
Sulfur mustard photodegradation

ABSTRACT

The photocatalytic decomposition of sulfur mustard (bis(2-chloroethyl)sulfide) has been examined on Fe-, Mn- and V-doped dispersed titania-silica catalysts. The catalysts were prepared by successive incipient wetness impregnation. They have been characterized by means of vibrational (FTIR) and optical (UV–vis–NIR in the DRS mode) spectroscopy. Powder XRD, XPS, and BET were used to characterize the structural morphology and texture. The reaction was carried out in two different types of reactors under both UV and visible light irradiation. The parent titania-silica catalyst showed activity only under UV irradiation, while the doped ones were active in the decontamination of the persistent sulfur mustard even under visible light irradiation.

1. Introduction

The decomposition of the real chemical warfare agents is of great interest as response to emerging situations in the case of a terrorist attack and also an alternative technology for chemical warfare agent existing stockpiles destruction. From the viewpoint of the mechanism of the reactions involved, decontamination of sulfur mustard is a complicated process, which is difficult to carry out [1]. A common belief is that nearly each decontaminant that destroy sulfur mustard efficiently can be used to decontaminate nearly any other chemical warfare agent.

In the last years it was revealed that the photocatalysis technique had a favourable potential to mineralize a range of toxic substances, and was regarded as a most promising technology to purify the polluted environment. Attempts to use the photocatalysis technique to detoxify chemical warfare agents and their simulants demonstrated this method to be principally feasible. Photocatalytic oxidation of sulfur mustard [2,3] and mustard gas simulant (organosulfur compounds) [4–12] over titania catalysts has been studied in the past decade.

The TiO_2/SiO_2 catalyst has been considered as an advanced material to replace pure titania, since it exhibit different surface chemical and photochemical properties as compared to TiO_2 itself [13]. Highly dispersed TiO_2 particles on high surface area SiO_2 possess high photooxidation as well as photoreduction capabilities [13]. The interface interaction leads to the formation of Ti–O–Si bonds strongly modifying the electron structure of the Ti atoms [14]. The dispersion of the material is closely related to the concentration of hydroxyl groups on the silica surface and the preparation conditions [15].

In a previous paper [16] we presented results on the photodecomposition activity in destroying such compounds using photocatalysts prepared by sol–gel method.

In this paper we present results on the photodegradation of sulfur mustard using titania-silica and titania-silica doped with Mn, Fe or V photocatalysts prepared by incipient wetness impregnation technique. The scope of this study was to verify if a more versatile preparation route as it is the incipient wetness impregnation is leading to the same performances and to investigate the characteristics of the new photocatalysts. The photocatalytic behaviour has been checked under both UV and visible light irradiation conditions, looking for the correlation between the electronic properties of the catalysts and their intrinsic behaviour.

2. Experimental

2.1. Photocatalysts preparation

The investigated modified titania-silica systems were prepared by incipient wetness impregnation of silica with titanium

* Corresponding author. Tel.: +40 21 4100241; fax: +40 21 4100241.
E-mail addresses: vasile.parvulescu@g.unibuc.ro (V.I. Pârvulescu), silvia.bordiga@unito.it (S. Bordiga), adriano.zecchina@unito.it (A. Zecchina).
[1] Fax: +39 0116707855.

0926-3373/$ – see front matter © 2009 Elsevier B.V. All rights reserved.
doi:10.1016/j.apcatb.2009.06.026

precursor followed by a re-impregnation procedure with a metal precursor. The silica support used for this study was Cabosil M-5 which was supplied from Riedel-de Haën. This material was treated with water in order to condense its volume for easier handling. The wet SiO_2 was dried at 393 K in order to remove the physical adsorbed water before impregnation. The base 5 wt.%. TiO_2/SiO_2 supported oxide catalyst was prepared by the incipient wetness impregnation of SiO_2 with an ethanol solution of titanium isopropoxide ($Ti(i\text{-}OC_3H_7)_4$, Aldrich, 97% purity). After impregnation at room temperature, the sample was kept overnight under N_2 flow. The sample was subsequently dried at 393 K for 2 h and calcined at 773 K in flowing air for 5 h. In the second step the 5 wt.% TiO_2/SiO_2 support was impregnated with a second species leading to 1 wt.% M/5 wt.% TiO_2/SiO_2 doped catalysts (M = Fe, Mn, and V). The impregnation was carried out using ethanol solutions of 15 wt.% of transition metal salts (Fe(III)acetylacetonate, Mn(II)acetylacetonate, and $VO(OC_3H_7)_3$). The removal of the solvent was carried out by conventional drying, first at room temperature for 24 h, and after that at 393 K for 2 h. Removal of residual organics and thermal stabilization of the materials was carried out by calcination for 5 h at 773 K in air atmosphere. The resulted photocatalysts were denoted as TiO_2/SiO_2 and $M/TiO_2/SiO_2$, where M is Fe, Mn or V.

2.2. Photocatalysts characterization

The samples have been investigated by means of vibrational (IR) and optical (UV–Vis–NIR in the DRS mode). XRD, XPS, and BET were used to characterize the structure and texture of these materials. In particular, FTIR spectra were collected, at a 2 cm^{-1} spectral resolution, in transmission mode on a Bruker IFS 66 FTIR spectrometer, equipped with an MCT cryodetector. The samples, in the form of compressed self-supporting wafers, have been hosted inside a cell allowing *in situ* sample activation (done at 773 K in vacuum) and gas dosage to be made at liquid-nitrogen temperature. Carbon monoxide (>99.997% purity) used as probe molecule in the investigation of the samples was supplied by Linde Italy. Because of the weakness of the interaction with CO, adsorption was studied at low temperature. Spectra were recorded at the nominal temperature of liquid nitrogen, by dosing increasing amounts of CO, in the 0.05–15 mbar equilibrium pressures range, on samples previously out-gassed. After each experiment, an evacuation step was performed, to study the reversibility of the interaction. Diffuse reflectance spectra (DRS) in the range of 200–2500 nm were taken on a PerkinElmer Lambda 19 spectrophotometer. The spectra were recorded against $BaSO_4$ as the baseline. The computer processing of the spectra with Bio-Rad Win-IR software consisted of conversion of wavelength (nm) to wavenumber (cm^{-1}) and calculation of the Kubelka–Munk function $F(R)$ from the absorbance. Samples were granulated for DRS measurements, and the size fraction of 60–100 mesh was loaded in a quartz cell with a Suprasil window. The spectra of the samples were obtained under ambient conditions. The band-gap energy (E_g) for allowed transition was determined by finding the intercept of the straight line in the low-energy rise of a plot of $[F(R)\cdot h\nu]^2$ against $h\nu$, where $h\nu$ is the incident photon energy [17]. Powder X-ray diffraction (XRD) patterns were recorded on a Siemens D 5000 diffractometer using the Cu Kα radiation (wavelength 1.5406 Å). The patterns were collected ranging 2θ from 5 to 70° with a step size of 0.1° and a time step of 1.0 s. XPS spectra were recorded at room temperature using a SSX-100 spectrometer, Model 206 from Surface Science Instrument. The pressure in the analysis chamber during the analysis was 1.33 mPa. Monochromatized Al-Kα radiation ($h\nu$ = 1486.6 eV) was used. It was generated by bombarding the Al anode with an electron gun operated with a beam current of 12 mA and acceleration voltage of 10 kV. The spectrometer energy scale was calibrated using the Au $4f_{7/2}$ peak centred at 83.98 eV. Charge correction was made with the C 1 s signal of adventitious carbon (C–C or C–H bonds) located at 284.8 eV. An estimated error of ±0.1 eV can be assumed for all measurements. Adsorption measurements were performed with a Micromeritics ASAP 2020 sorption analyzer. Surface areas have been obtained by N_2 adsorption at the nominal temperature of liquid nitrogen (~77 K) on all materials previously out-gassed at 473 K in vacuum. The specific surface areas and the pore size distributions were calculated from the Brunauer–Emmett–Teller (BET) equation [18] and from the desorption isotherm using the Barrett–Joyner–Halenda (BJH) method [19], respectively.

2.3. Photocatalytic tests

For the photo-decomposition of sulfur mustard, the catalytic tests have been carried out under both UV and visible light irradiation. A detailed description of the experimental procedure and photocatalytic reactors is given in a previous work [16]. In summary, two types of quartz reactors (an open reactor naturally aerated and a closed tube in which a constant flow of air was introduced) and two types of irradiation sources were used. As UV irradiation source a 125 W high-pressure germicidal black-bulb lamp (HQV 125 W, Osram, Germany) with a maximum emission at 365 nm, 3.0 W UVA radiated power 315–400 nm and 810 lx light intensity was used. Photodegradation tests under visible light irradiation were carried out in the same reactors using a 200 W Ne lamp (F74-765, Tungsram, Hungary) with a maximum emission at 600 nm and light intensity of 4300 lx. Light intensity at the distance where the sample was placed was measured in both cases with an 840,006 Speer Scientific luxmeter. Sulfur mustard (bis(2-chloroethyl)sulfide) was prepared by the Meyer method and distilled at 383 K [20]. *Caution*: *sulfur mustard is a potent vesicant and must be handled only by trained personnel using safety procedures in a closed system or in a hood under good ventilation.* A general photocatalytic procedure was carried out as follows: 20 mg of photocatalyst to which 100 μL 0.77 wt.% solution of sulfur mustard in CH_2Cl_2 were added are placed into an open polyethylene vat. The ensemble has been introduced in the above reactors. For the sake of comparison, in all the photocatalytic tests TiO_2 Degussa P25 was used as reference. Samples of the gas phase inside the closed reactor were taken at regular intervals with a gas-tight syringe and analyzed using a GC/MS equipment Saturn 2100 T from Varian. The chromatograph was calibrated for sulfur mustard, carbon dioxide, sulfur dioxide, bis(2-chloroethyl)disulfide, acetaldehyde, and chloroethylene. The calibration was performed by injection of the mixtures of the respective gases with air into the GC–MS equipment. The evolution of the reaction was also followed by taking the content of the vat at the required reaction time, washing the catalyst with CH_2Cl_2, concentrating and analyzing the resulting solution using the same GC/MS equipment.

3. Results and discussion

3.1. Photocatalysts characterization

3.1.1. XRD characterization

All the prepared photocatalysts were amorphous as it resulted from the XRD patterns (not shown here). Except the boss in the range 2θ 25–30 assigned to the amorphous silica support, no other reflection plane has been identified.

3.1.2. FTIR Spectroscopy

Fig. 1 reports spectra of TiO_2/SiO_2 and $M/TiO_2/SiO_2$ (M = Fe, Mn, V) out-gassed at 773 K, normalized to unit weight in order to allow the comparison. All spectra exhibit a sharp strong band at 3747 cm^{-1} due to stretching vibrations of the isolated (non-

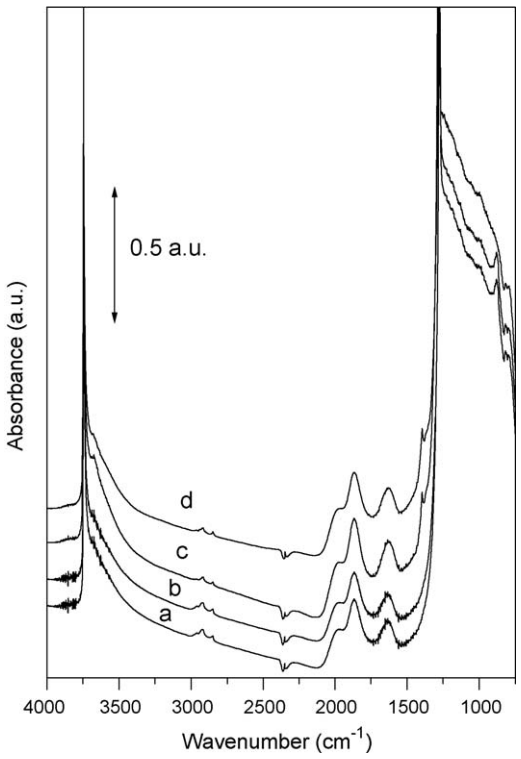

Fig. 1. FTIR spectra of (a) TiO_2/SiO_2, (b) $Mn/TiO_2/SiO_2$, (c) $V/TiO_2/SiO_2$, and (d) $Fe/TiO_2/SiO_2$ photocatalysts.

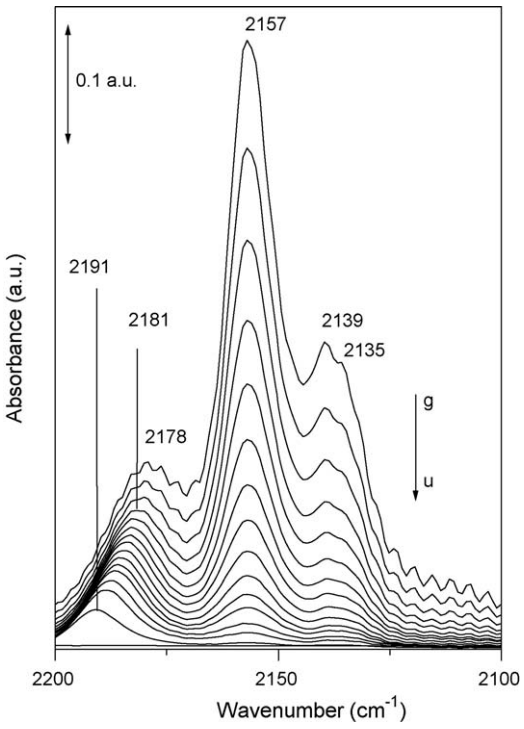

Fig. 2. FTIR spectra of the 2200–2100 cm^{-1} region of CO adsorbed at 77 K on TiO_2/SiO_2 sample. Initial equilibrium pressure of 15 mbar, followed by evacuation at different pressures (spectra g–u).

interacting) surface silanols and a broad tail in the low frequency side due to hydrogen bonded silanols. The spectra are very similar and nearly identical to those of silica out-gassed at the same temperature (not reported for simplicity). This result indicates that the samples cannot be differentiated *via* examination of the hydroxyl groups stretching region and that the contribution of M–OH groups (M = Ti, V, Fe, Mn), if any, cannot be singled out. Examination of the 1000–850 cm^{-1} region, where the stretching modes of Si–O–M groups is expected [21,22] to occur, do not show remarkable differences between the four examined samples.

3.1.3. Low-temperature CO adsorption

The properties of surface sites on doped titania-silica catalysts have been examined through the use of specific probe molecules. CO adsorption can be used to characterize both acidic and basic sites of metal oxides. Adsorption of carbon monoxide on the investigated samples at the nominal temperature of liquid nitrogen (~77 K) (15 mbar maximum equilibrium pressure) resulted in the appearance of three principal bands in the carbonyl stretching region, their maxima being located at 2178, 2157 and 2139 cm^{-1} (Fig. 2). The bands are all reversible upon lowering the equilibrium pressure Figs. 2–5 depicts the evolution of the spectra of adsorbed CO upon gradually decreasing the equilibrium pressure.

The pressure decrease led to a progressive disappearance of the bands at 2135, 2139 and 2178 cm^{-1}. The reversibility is always in the order: 2135 > 2139 > 2178 cm^{-1}. The complex absorption at 2138 cm^{-1} is undoubtedly due to physically adsorbed CO. In agreement with literature data the peak at 2157 cm^{-1}, present on all samples and on pure silica, is assigned to CO hydrogen bonded to silanols [23,24]. The frequency of the peak is not influenced by the coverage. The appearance of the 2157 cm^{-1} band is accompanied by the erosion of the 3747 cm^{-1} peak with formation of a broader feature at 3662 cm^{-1} assigned to hydroxyl groups perturbed by hydrogen bonding (spectra not shown for brevity).

The original 3747 cm^{-1} band is restored upon decreasing the CO pressure as expected. In conclusion the Brönsted acidity of the sample is determined by the surface silanol groups. Many data in the literature point out that the shift of ν(OH) for surface silanols, observed upon CO adsorption, is around −90 cm^{-1} [23,24]. The shift measured in this case, namely −85 cm^{-1} is in a typical range. The band at 2181–2191 cm^{-1}, not observed on pure silica and present on all samples, is attributed to CO adsorbed on Ti^{4+} centres present on the surface of small TiO_2 particles supported on silica. The frequency, 35–48 cm^{-1} upward shifted with respect to CO gas, indicates that the surface Ti^{4+} centres are coordinatively unsaturated and displace Lewis acidity.

Unlike the other bands at 2157 and 2138 cm^{-1}, the peak at 2178 cm^{-1} gradually shifts with coverage and reaches the 2191 cm^{-1} value at $\theta \rightarrow 0$. This shift is indicative of adsorbate–adsorbate interactions (both static and dynamic) [25,26] between CO parallel oscillators adsorbed on flat terraces and facelets of TiO_2 microcystals. This result also indicates that the adsorption sites cannot be described as isolated Ti^{4+} cations grafted on the silica support.

The comparison of the spectra reported in Figs. 2–4 show that the CO probe is not able to give information about the presence of $M^{x+}(CO)$ (M = V, Mn) species. This can be due to the following facts: (i) the frequency of the bands of these species are coincident with the frequency of band of $Ti^{4+}(CO)$ complexes and hence are fully overshadowed; (ii) the surface area of the supported vanadium and manganese oxides is very low. The two explanations are not in conflict.

The situation is definitely different when the spectrum of CO adsorbed on $Fe/TiO_2/SiO_2$ is considered. In fact in this case a new weak peak is definitely observed at 2170 cm^{-1} for lowest coverages which can be assigned to CO adsorbed on Fe^{3+} centres located on TiO_2 particles. This tentative assignment is in agreement with the observation that this peak is not present on Fe/SiO_2 system (result not shown for brevity).

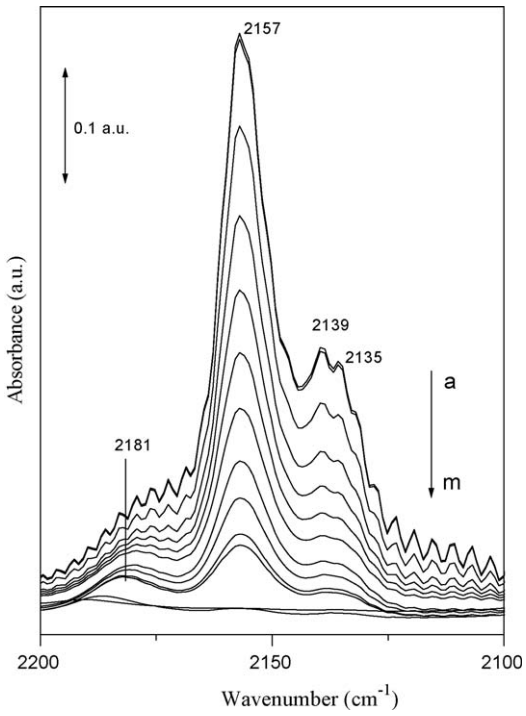

Fig. 3. FTIR spectra of the 2200–2100 cm^{-1} region of CO adsorbed at 77 K on Mn/TiO_2/SiO_2 sample. Initial equilibrium pressure of 15 mbar, followed by evacuation at different pressures (spectra a–m).

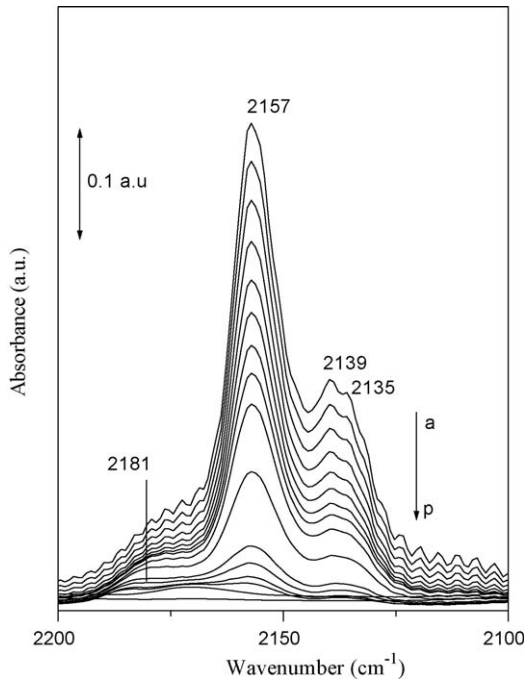

Fig. 5. FTIR spectra of the 2200–2100 cm^{-1} region of CO adsorbed at 77 K on Fe/TiO_2/SiO_2 sample. Initial equilibrium pressure of 15 mbar, followed by evacuation at different pressures (spectra a–p).

Some indirect information about the state of dopant oxides can be obtained by inspection of the 2178–2191 cm^{-1} region characteristic of CO on TiO_2 particles. In fact an intensity decrement of this absorption is observed on all samples, the effect being particularly remarkable for the Fe/TiO_2/SiO_2 and Mn/TiO_2/SiO_2 samples. This is strong indication that the dopant oxides are covering the surface of titania particles and that the effect is particularly relevant on Fe/TiO_2/SiO_2 system. This behaviour could be tentatively justified as follows: (i) VO_x, which is an active acidic oxide, usually anchor to the oxide support by preferentially titrating the basic surface hydroxyls of oxide support (TiO_2 in our case) [27]; (ii) the basic oxide FeO_x can anchor to the oxide substrate by preferentially titrating the surface Lewis acid sites of the support [28,29]; (iii) the same can occur with MnO_x, which is also an active basic oxide. In our opinion, on the basis of these IR data no more detailed information about the state of the dopant oxides can be inferred.

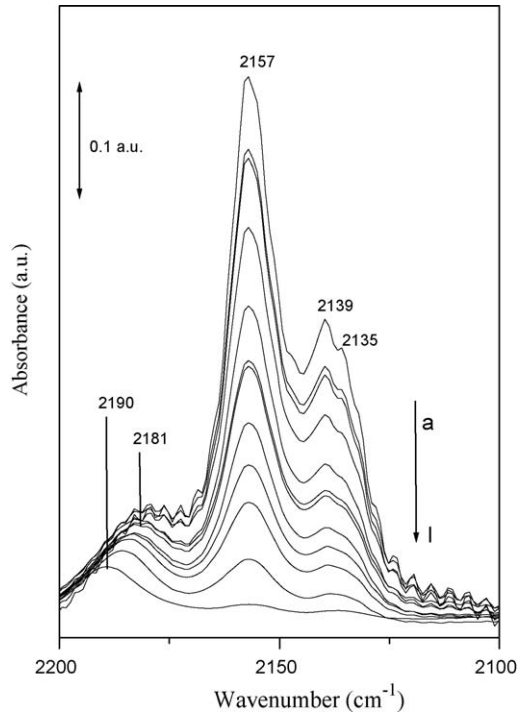

Fig. 4. FTIR spectra of the 2200–2100 cm^{-1} region of CO adsorbed at 77 K on V/TiO_2/SiO_2 sample. Initial equilibrium pressure of 15 mbar, followed by evacuation at different pressures (spectra a–l).

3.1.4. Adsorption measurements and X-ray photoelectron spectroscopy (XPS) surface analysis

Table 1 compiles the surface areas for the reference materials, the surface Ti/Si, M/Ti, M/Si (M= Fe, Mn, V) XPS atomic ratios and the corresponding binding energies of the Si 2p, Ti $2p_{3/2}$, O 1s, and M $2p_{3/2}$ (M = Fe, Mn, and V) levels. All materials exhibited surface areas comparable with their corresponding supports. Upon calcination at 773 K, for the TiO_2/SiO_2 catalyst, a sintering effect occurred and the surface area decreased. Based on the fact that following the preparation procedure almost all the TiO_2 is located on outer surface of the material the fraction of the surface area corresponding to TiO_2 is around 19%. After the dopant metal oxide deposition, the surface area of the titania-silica supports further decreased. This effect can be explained by an additional blockage of pores due to the formation of the metal oxide layer and/or structural changes occurring during the heat treatment. XPS spectra of the reference materials are compared to that of pure titania consisting of anatase and silica Cabosil M-5. For all the samples the binding energy of the Ti $2p_{3/2}$ level corresponds to the Ti^{4+} oxidation state [30–33].

The binding energies of the doping metals fit very well with the values of V^{5+} in V_2O_5, Fe^{3+} in Fe_2O_3, and Mn^{4+} in MnO_2, respectively [34]. The pure titania shows a binding energy of 458.5 eV, indicating that the titanium ions in the anatase lattice are

Table 1
Surface area, surface composition, and the binding energies of core electrons for the reference materials.

Sample	S_{BET} (m^2/g)	Ti/Si XPS atomic ratio	M/Ti XPS atomic ratio	M/Si XPS atomic ratio	B.E. (eV)			
					Si 2p	Ti $2p_{3/2}$	O 1s	M $2p_{3/2}$
TiO_2 anatase	57					458.5	530.7	
TiO_2/SiO_2	277	0.376			104.1	459.8	533.1	
$Fe/TiO_2/SiO_2$	211	0.240	0.141	0.034	104.0	459.9	533.4 (95)[a] 530.6 (5)	711.3
$Mn/TiO_2/SiO_2$	265	0.260	0.350	0.091	103.8	459.6	533.0 (95) 530.5 (5)	642.4
$V/TiO_2/SiO_2$	241	0.474	0.988	0.468	103.9	459.5	533.1 (90) 530.5 (10)	517.2
SiO_2	330				103.4		532.9	

[a] The number presented in parentheses indicates the percentage of the band.

surrounded octahedrally by oxygen ions. In contrast, the reference materials exhibit upward shifts of titanium and oxygen binding energies, which could be associated with the isolated TiO_4 sites that possess maximum number of Ti–O–Si bonds per Ti atom. This result is associated to an increase in the effective positive charge on Ti since the Si atoms are more electronegative and less polarisable than the Ti atoms [13]. In the case of the doped photocatalysts, besides the band of O 1s at ~533.1 eV, which is due to the oxygen of the SiO_2 support, a second band arisen at ~530.5 eV. The relative percentage of this new O 1s increases with metal oxide loading suggesting that this new peak is associated to the dispersed dopant species. The Ti/Si ratio changed strongly with the impregnation step. Both M/Ti and M/Si ratios indicate an excellent homogeneity of these catalysts. As mentioned above the spectral data suggest that the vanadia was deposited preferentially on titanium sites, indicating the higher affinity of the vanadium precursor for reacting with Ti–OH groups compared to Si–OH groups. A possible explanation for the higher dispersion of the vanadia species is their higher mobility on the titania surface at elevated temperature [13].

3.1.5. The UV–Vis–NIR diffuse reflectance spectroscopy

The DRS spectra of the reference materials are presented in Fig. 6. In the UV–vis region, the TiO_2/SiO_2 sample possesses an absorption threshold at ~335 nm (3.70 eV), which is characteristic of the transition between the valence and conduction band of TiO_2 particles. The UV–vis spectra of $V/TiO_2/SiO_2$ sample exhibits an absorption threshold at ~375 nm (3.31 eV). This shift is presumably due to the superposition of the TiO_2 and VO_x interband absorptions. No distinct d–d transitions, typical for the presence of reduced vanadium oxide species can be observed: this result is indicating that vanadium was mainly present in its highest oxidation state. The shift of the absorption edge in the case of $Fe/TiO_2/SiO_2$ sample is more remarkable in agreement with the fact that the edge of iron oxides is occurring at lower frequencies. The broad and weak band that appears at ~570 nm can be ascribed to the $^2T_{2g} \rightarrow {}^2A_{2g}$ d–d transitions of dopant Fe^{3+} in small oxide particles highly dispersed on TiO_2 [35]. The spectrum of $Mn/TiO_2/SiO_2$ presents also a remarkable shift of the absorption edge (band-gap energy shifted to 3.6 eV) which could be interpreted as due to dispersed manganese oxide.

In the near-IR region (Fig. 7) where the overtone and combination bands of hydroxyls are located, the spectra show bands at 7310, 7131, 6855, and 5260 cm^{-1}. The 7310 cm^{-1} band can be assigned to the overtone vibration of the isolated Si–OH groups at 3747 cm^{-1} [36]. The 2ν overtone band of isolated Si–OH hydroxyls at 7310 cm^{-1} for the TiO_2/SiO_2 and $M/TiO_2/SiO_2$ (M = V, Fe and Mn) samples is influenced by the metal loading. This band increases when transition metal oxides are added. It should be noticed that the addition of metal oxides to the TiO_2/SiO_2 support consumes some of the remaining surface Si–OH hydroxyls. This is a proof the surface metal oxide species also interact with the silica surface. The bands at 7131, 6855, and 5260 cm^{-1} can be associated with physisorbed H_2O molecules on the sample surface under ambient conditions.

3.2. Photocatalytic behaviour

In the case of photo-decomposition of sulfur mustard we have performed a series of blank experiments. These experiments were done in order to prove that this reaction is a photocatalyzed process. Prior to determining the photocatalytic activity of the investigated materials, adsorption experiments were carried out. These experiments were performed to differentiate between physisorption and the real photocatalytic process. Thus, the catalysts were kept for 15 min in dark conditions, and the analysis of the liquid phase revealed the disappearance of sulfur mustard with a maximum of about 15% for the TiO_2/SiO_2 material. After percolation with CH_2Cl_2, all the adsorbed molecules have been completely recovered, which means that the decrease in sulfur mustard corresponded only to physisorption of the vesicant agent onto catalyst surface and not to a real photocatalytic process. These experiments demonstrate that under the investigated catalysts and temperature conditions no dark reaction occurs. Also, photo-

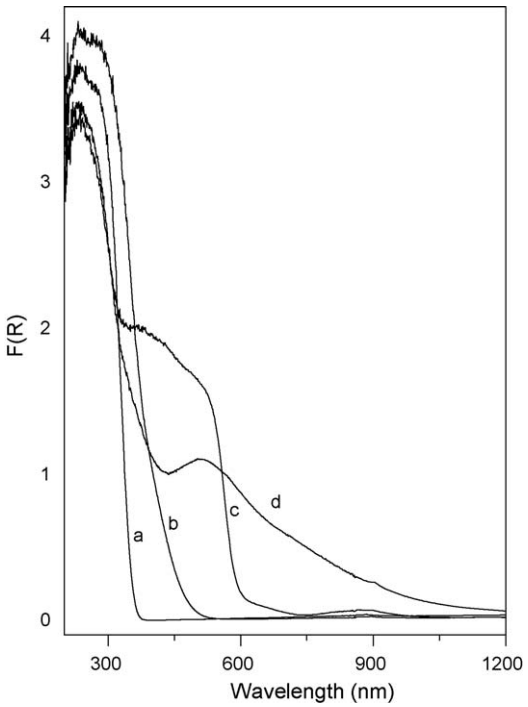

Fig. 6. UV–vis DRS spectra of the reference materials: (a) TiO_2/SiO_2, (b) $V/TiO_2/SiO_2$, (c) $Fe/TiO_2/SiO_2$, and (d) $Mn/TiO_2/SiO_2$.

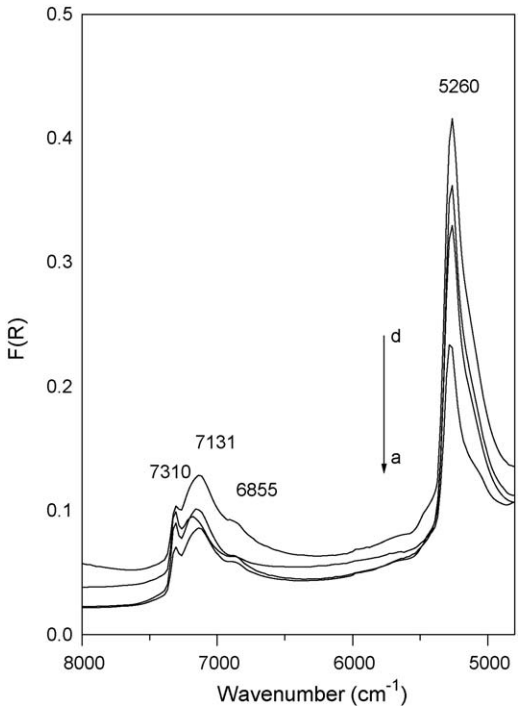

Fig. 7. NIR DRS spectra of the reference materials: (a) TiO_2/SiO_2, (b) $V/TiO_2/SiO_2$, (c) $Fe/TiO_2/SiO_2$, and (d) $Mn/TiO_2/SiO_2$.

exposure of sulfur mustard in the absence of the catalyst was not accompanied by any decomposition. When the TiO_2 Degussa P25 reference material was used, after 2 h of UV light exposure, no significant degradation process has been observed. It is possible that, because of a small surface area, TiO_2 is not capable to efficiently adsorb larger quantities of chemical warfare agent and so its photocatalytic activity is low. The presence of a second phase with good adsorptive capabilities (like the SiO_2 support) led to better photocatalytic results. This result induces the idea of an excellent synergism between the photocatalyst and the support. Such a behaviour has been observed also in the case of a TiO_2-activated carbon system [37].

The photocatalytic decomposition reaction of sulfur mustard led to the formation of the same gaseous products irrespective of the investigated catalysts. The gaseous products are chloroethylene, carbon dioxide, sulfur dioxide, and bis(2-chloroethyl)disulfide. The evolution of the photocatalytic decomposition at different reaction time (1 and 2 h) was followed by washing the catalyst with CH_2Cl_2, concentrating and analyzing the resulting solution. The surface extract contain only bis(2-chloroethyl)disulfide. Other products (such as sulfates) which are produced in the last stage of sulfur mustard oxidation were not detected in our experiments.

The photocatalytic reaction begins only after switching on the lamp. The photoexcitation of titania generates an electron–hole pair, creating the potential for both reduction and oxidation processes to occur at the surface of the photocatalyst. Although a number of possible degradation pathways can be envisioned, the formation and subsequent reactions of hydroxyl radicals, generated from the oxidation of water molecules by photoexcited titania, are generally accepted as the predominant degradation pathways of organic substrates.

An increase in the band-gap of the TiO_2 particles has been ascribed to an elevation of the conduction band edge as well as the lowering of the valence band edge. Thus, the electronic properties are changed due to the increased band-gap energy. The oxidizing potential of the photon generated holes and the reducing potential of the photon generated electrons will increase with increasing

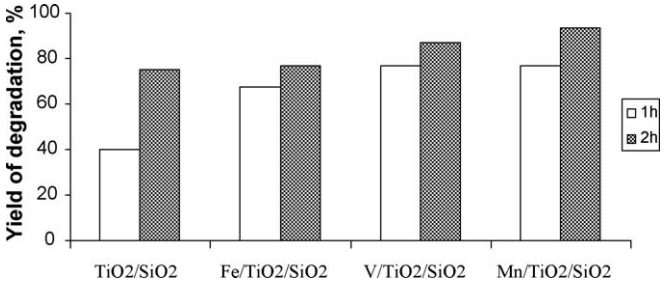

Fig. 8. Photocatalytic degradation percent of sulfur mustard under normal atmosphere (air flux 50 cm^3/min air; catalyst 20 mg; UV irradiation; irradiation time 1 and 2 h in the photoreactor with a controlled air flow).

band-gap. In addition to the improved oxidizing and reducing abilities, some synergism between the TiO_2 and SiO_2 phases has been observed. The photogenerated intermediate oxidants on the TiO_2 sites, such as hydroxyl radical ($HO^{\bullet}$) or species from reduction of O_2 ($HO_2^{\bullet}$), must diffuse and react with sulfur mustard molecules on the SiO_2 sites. The increased oxidizing potential of the Ti cations, due to the formation of Ti–O–Si bonds, is also reflected by the increased binding energy value of Ti $2p_{3/2}$ and the higher ligand–metal charge–transfer transitions of the Ti atoms in the TiO_2/SiO_2 catalysts.

Figs. 8 and 9 present the results of photo-decomposition of sulfur mustard in the presence of the photocatalysts after 1 and 2 h of exposure to UV irradiation using both type of experimental set-up. As it could be observed, the $M/TiO_2/SiO_2$ catalysts produce a higher yield of degradation then undoped titania-silica material, irrespective of the experimental set-up. We could note that the $Fe/TiO_2/SiO_2$ material is active in the photodegradation of sulfur mustard, but with a much lower efficiency, due to the significantly lower surface area or to a high recombination rate of photo-generated electron–hole pairs. Also, the photo-decomposition efficiency of $Mn/TiO_2/SiO_2$ and $V/TiO_2/SiO_2$ is comparable with a yield of degradation bigger than 85% in both cases.

The high rate observed in the photo-decomposition of sulfur mustard on Mn-doped sample could be correlated with the role played by exposed Mn species on the surface of the TiO_2/SiO_2 support in speeding up the activity of the photocatalyst by releasing electrons and holes under irradiation. The photogenerated e^-/h^+ pairs can easily and quickly diffuse to the surface of catalysts to form active sites at which photocatalytic reactions are produced. More specifically, in $Mn/TiO_2/SiO_2$, the photogenerated electrons transfer from TiO_2 to Mn particles and the holes remain on the TiO_2, resulting in charge separation of the photo-formed e^-/h^+ pairs with good efficiency.

All photocatalysts were also tested under vis light irradiation. Figs. 10 and 11 summarises the results of photo-decomposition of sulfur mustard in the presence of the photocatalysts after 1 and 2 h

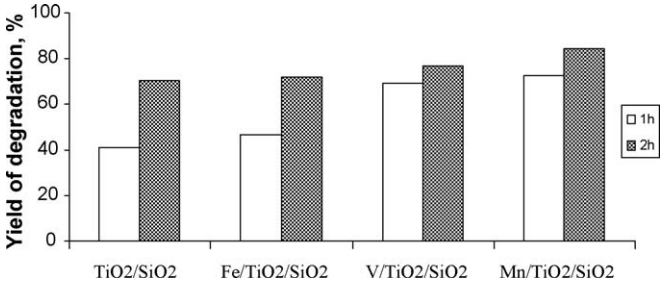

Fig. 9. Photocatalytic degradation percent of sulfur mustard under normal atmosphere (catalyst 20 mg; UV irradiation; irradiation time 1 and 2 h in the photoreactor with constant oxygen concentration).

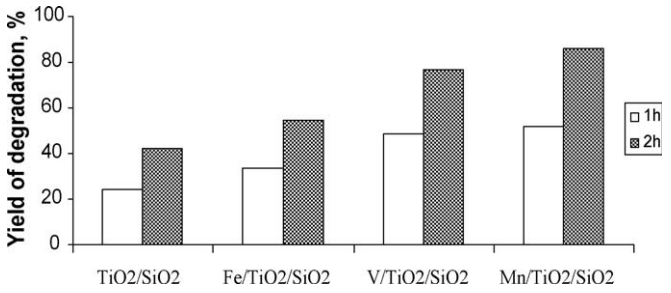

Fig. 10. Photocatalytic degradation percent of sulfur mustard under normal atmosphere (air flux 50 cm^3/min air; catalyst 20 mg; vis irradiation; irradiation time 1 and 2 h in the photoreactor with a controlled air flow).

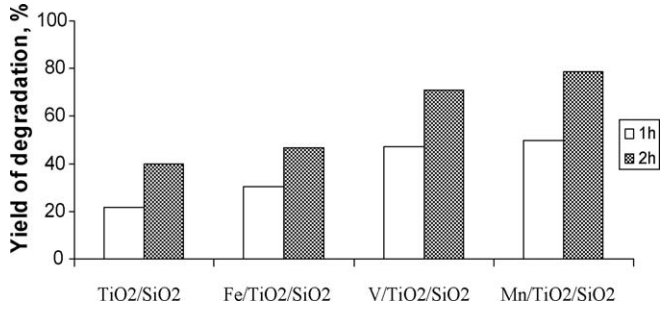

Fig. 11. Photocatalytic degradation percent of sulfur mustard under normal atmosphere (catalyst 20 mg; vis irradiation; irradiation time 1 and 2 h in the photoreactor with constant oxygen concentration).

of exposure to visible light irradiation using both type of experimental set-up.

Under visible light irradiation the yield of degradation decreases of about 10–15% and the distribution of the reaction products remain unchanged. As in the case of the photocatalytic decomposition under UV irradiation, the most active catalysts were again Mn and V doped titania-silica materials. It should be noticed that TiO_2/SiO_2 photocatalyst presents the lowest photoactivity. This behaviour could be only be partially explained by a relation between the reaction rate and the used wavelength because, on this basis, the $Fe/TiO_2/SiO_2$ system should show an activity intermediate between that of $Mn/TiO_2/SiO_2$ and that of $V/TiO_2/SiO_2$. For the TiO_2/SiO_2 photocatalyst only few percents of the light radiation are used by the catalyst to produce the photodecomposition of sulfur mustard. Even that, the adsorption capabilities of this material is enough to lead to a yield of degradation of about 40%. In conclusion, compared to the parent TiO_2/SiO_2 photocatalyst, the doping with the investigated elements allows this reaction under visible light. Furthermore, under the investigated conditions, the yield of degradation reached almost 90% that is indeed remarkable. Fig. 12 gives the reaction mechanism on the investigated catalysts. In order to have an idea about the kinetics of photodegradation of sulfur mustard over titania-silica photocatalysts several experiments have been performed. The kinetics experiments are presented in Fig. 13. These plots indicate that the photodegradation follows a pseudo-first order kinetics for all doped titania-silica photocatalysts, while for the TiO_2/SiO_2 parent photocatalyst the degradation of sulfur mustard accounts to a pseudo-zero order kinetics. Finally these results show an additional very practical advantage. Comparing with the sol–gel route that is a complicate procedure for bulk materials, incipient wetness impregnation is a very facile one. Thus comparing with data reported previously [16], incipient wetness impregnation is leading to very comparable photocatalytic results. One of the reasons of this behaviour is the fact that, in this case, Ti

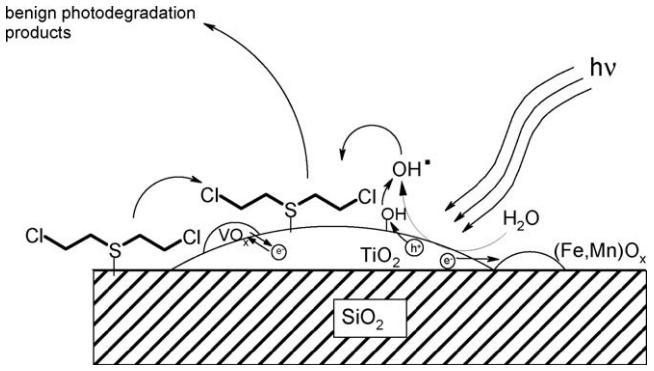

Fig. 12. Proposed mechanism for photodegradation of sulfur mustard over $M/TiO_2/SiO_2$ photocatalysts.

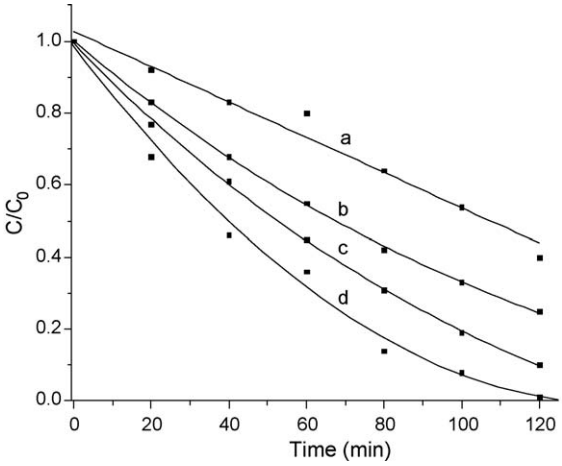

Fig. 13. Kinetics of photocatalytic degradation of sulfur mustard under UV irradiation on TiO_2/SiO_2 (a), $Fe/TiO_2/SiO_2$ (b), $V/TiO_2/SiO_2$ (c), and $Mn/TiO_2/SiO_2$ (d) photocatalysts.

atoms are mostly located on the outer surface of the silica support, in contrast with the sol–gel TiO_2-SiO_2 systems where an important part of titanium is dispersed in the silica matrix.

4. Conclusion

Mn, Fe and V doped TiO_2/SiO_2 photocatalysts were investigated in the decomposition of sulfur mustard under both UV and visible light irradiation. The results obtained combining XRD, FTIR, XPS, and UV–vis–NIR DRS and low-temperature CO adsorption provided an advanced characterization of the surface structures of the dispersed TiO_2/SiO_2 and $M/TiO_2/SiO_2$ supported oxides. They confirmed that the materials used in this study are promising for the photo-decontamination of sulfur mustard as they are leading to a destruction of this agent in a relatively short time, under visible irradiation. While TiO_2/SiO_2 is active only under UV irradiation, the doped $M/TiO_2/SiO_2$ photocatalysts can efficiently operate even under visible and/or solar light irradiation. These results encourage the synthesis of new modified titania-silica systems which could be used in the decontamination of the persistent chemical warfare agents.

Acknowledgments

The authors kindly acknowledge NATO's Scientific Affairs Division in the framework of the Science for Peace Programme Sfp 981476 for the financial support. This research has also been

partially supported by the CNCSIS through the PN-II-RU-TD-2007-1 project (contract number 20/2007) supervised by Ştefan Neaţu.

References

[1] G.-M. Zuo, Z.-X. Cheng, G.-W. Li, L.-Y. Wang, T. Miao, Environ. Sci. Technol. 39 (2005) 8742.
[2] B. Cojocaru, V.I. Parvulescu, E. Preda, G. Epure, V. Somoghi, E. Carbonell, M. Alvaro, H. Garcia, Environ. Sci. Technol. 42 (2008) 4908.
[3] M. Grandcolas, A. Louvet, N. Keller, V. Keller, Angew. Chem. Int. Ed. 48 (2009) 161–164.
[4] R.S. Davidson, J.E. Pratt, Tetrahedron Lett. 24 (1983) 5903.
[5] L.C. Cerny, Y.-C. Yang, J.R. Ward, In Proceedings of the 1988 Scientific Conference on Chemical Defense Research, CRDEC-SP-013; U.S. Army CRDEC: Aberdeen Proving Ground, MD, May 1989; Vol. 1, pp. 83.
[6] M.A. Fox, Y.–S. Kim, A.A. Abdel-Wahab, M. Dulay, Catal. Lett. 5 (1990) 369.
[7] A.V. Vorontsov, E.V. Savinov, L. Davydov, P.G. Smirniotis, Appl. Catal. B: Environ. 32 (2001) 11.
[8] A.V. Vorontsov, L. Davydov, E.P. Reddy, C. Lion, E.N. Savinov, P.G. Smirniotis, New J. Chem. 26 (2002) 732.
[9] D.V. Kozlov, A.V. Vorontsov, P.G. Smirniotis, E.N. Savinov, Appl. Catal. B: Environ. 42 (2003) 77.
[10] I. Martyanov, K.J. Klabunde, Environ. Sci. Technol. 37 (2003) 3448.
[11] D.A. Panayotov, D.K. Paul, J.T. Yates Jr., J. Phys. Chem. B 107 (2003) 10571.
[12] D. Panayotov, P. Kondratyuk, J.T. Yates Jr., Langmuir 20 (2004) 3674.
[13] X. Gao, I.E. Wachs, Catal. Today 51 (1999) 233.
[14] R.W. Matthews, J. Catal. 113 (1988) 549.
[15] S. Haukka, E. Lakomaa, A. Root, J. Phys. Chem. 97 (1993) 5085.
[16] S. Neatu, V.I. Parvulescu, G. Epure, E. Preda, V. Somoghi, A. Damin, S. Bordiga, A. Zecchina, Phys. Chem. Chem. Phys. 10 (2008) 6562.
[17] W.N. Delgass, G.L. Haller, R. Kellerman, J.H. Lunsford, Spectroscopy in Heterogeneous Catalysis, Academic Press, New York, 1979.
[18] S. Brunauer, P.H. Emmett, E. Teller, J. Am. Chem. Soc. 60 (1938) 309.
[19] E.P. Barrett, L.G. Joyner, P.P. Halenda, J. Am. Chem. Soc. 73 (1951) 373.
[20] S. Franke, Lehrbuch der Militärchemie, 1, Militärverlag der DDR, Berlin, 1977.
[21] AstorinoF E., J.B. Peri, R.J. Willey, G. Busca, J. Catal. 157 (1995) 482.
[22] A. Zecchina, S. Bordiga, C. Lamberti, G. Ricchiardi, C. Lamberti, G. Ricchiardi, D. Scarano, G. Petrini, G. Leofanti, M. Mantegazza, Catal. Today 32 (1996) 97.
[23] T.P. Beebe, P. Gellin, Y.T. Yates Jr., Surf. Sci. 148 (1984) 526.
[24] A. Zecchina, C. Lamberti, S. Bordiga, Catal. Today 41 (1998) 169.
[25] A. Tsyganenko, L. Denisenko, S. Zverev, V. Filimonov, J. Catal. 94 (1985) 10.
[26] A. Zecchina, D. Scarano, A. Reller, J. Chem. Soc. Faraday Trans. I 84 (1988) 2327.
[27] A.M. Turek, I.E. Wachs, E. DeCanio, J. Phys. Chem. 96 (1992) 5000.
[28] M.A. Vuurman, D.J. Stufkens, A. Oskam, I.E. Wachs, J. Chem. Soc. Faraday Trans. 17 (1996) 3259.
[29] M. de Boer, A.J. van Dillen, D.C. Koningsberger, J. Geus, M.A. Vuurman, I.E. Wachs, Catal. Lett. 11 (1991) 227.
[30] P. Wauthoz, M. Ruwet, T. Machej, P. Grange, Appl. Catal. 69 (1991) 149.
[31] G.B. Raupp, J.A. Dumesic, J. Phys. Chem. 89 (1985) 5240.
[32] S. Mukhopadhyay, S. Garofalini, J. Non-cryst. Solids 126 (1990) 202.
[33] Z. Wei, Q. Xin, X. Guo, E. Sham, P. Grange, B. Delmon, Appl. Catal. 63 (1990) 305.
[34] C.D. Wagner, W.M. Riggs, L.E. Davis, J.F. Moulder, G.E. Muilenberg (Eds.), Handbook of X-ray photoelectron Spectroscopy, Perkin-Elmer Corporation, Minnesota, 1979, p. 70, 74, and 76.
[35] C.J. Ballahausen, Introduction to Ligand Field Theory, McGraw–Hill, New York, 1962.
[36] E.F. Vansant, P.V.D. Voort, K.C. Vrancken, Stud. Surf. Sci. Catal. (1995) 93.
[37] B. Cojocaru, S. Neatu, V.I. Parvulescu, V. Somoghi, N. Petrea, G. Epure, M. Alvaro, H. Garcia, Chem. Sust. Chem. 2 (2009) 427.